ELSEVIER

Thin Solid Films 413 (2002) 212–217

thin solid films

www.elsevier.com/locate/tsf

Correlation between structural and magnetic properties of thin $Fe_xCo_{1-x}(1\,1\,0)$ films on sapphire

J. Swerts*, K. Temst, N. Vandamme, B. Opperdoes, C. Van Haesendonck, Y. Bruynseraede

Laboratorium voor Vaste-Stoffysica en Magnetisme, Katholieke Universiteit Leuven, Celestijnenlaan 200 D, B-3001 Leuven, Belgium

Received 16 July 2001; received in revised form 26 January 2002; accepted 28 February 2002

Abstract

Fe and $Fe_{40}Co_{60}$ thin films (5–60 nm) with a bcc structure have been prepared on *a*-axis oriented sapphire substrates by molecular beam epitaxy. The structural properties have been characterized in situ by reflection high-energy electron diffraction and ex situ by X-ray diffraction and atomic force microscopy. A two-dimensional magneto-optical Kerr effect set-up has been used to determine the in-plane magnetization components and to investigate the magnetic anisotropy and the orientation dependence of the magnetization reversal process. The Fe films and $Fe_{40}Co_{60}$ alloy films both display a uniaxial in-plane anisotropy. They also exhibit a comparable increase of the coercive field along the easy axis with increasing thickness. We have evaluated this dependence using the results of the structural characterization, indicating that the enhancement of the coercive field is linked to the growing surface roughness and decreasing structural coherence.

Keywords: Fe; FeCo alloys; Structural properties; Magnetic properties and measurements; Anisotropy

1. Introduction

There is at present considerable interest in the magnetic properties of the 3d transition metals and metal alloys, in particular in thin ferromagnetic films with controllable magnetic anisotropy, due to promising technological applications [1]. The Fe_xCo_{1-x} alloy is a fundamentally and technologically interesting ferromagnetic material because of its large variations in magnetic properties with composition. In bulk bcc Fe_xCo_{1-x} alloys, the first crystal anisotropy constant K_1 changes sign as the Co content increases [2]. Also in thin films this behaviour has been reported for Fe_xCo_{1-x} alloy films on ZnSe and MgO substrates [3,4].

The epitaxial growth and magnetic properties of bcc Fe are widely investigated and can be influenced by using different deposition techniques and various substrates [5]. Bulk Fe exists in the stable bcc phase under ordinary conditions. Related phases can be stabilized at room temperature using suitable substrates e.g. fct Fe can be stabilized by epitaxial growth on the Cu(1 0 0) surface [6], even hcp Fe has been reported [7]. In contrast to the stable bcc Fe, the structural bcc Co phase is metastable. Only on suitable substrates bcc Co can be stabilized e.g. on Cr(1 0 0) surfaces ultra-thin Co films could be grown in the metastable bcc phase [8]. The stability of bcc Fe_xCo_{1-x} alloys is dependent on the composition and the substrate. Fe_xCo_{1-x} alloys are in general only thermodynamically stable as bcc structure for $0.25 < x \leqslant 1$ [9]. Gutierrez et al. achieved a stable bcc phase of Fe_xCo_{1-x} over the entire range of alloy concentrations using ZnSe-epilayered GaAs substrates [3].

In this paper, we will focus on the ferromagnetic properties of the bcc Fe and bcc $Fe_{40}Co_{60}$ system grown on *a*-axis oriented sapphire substrates. When bcc Fe was grown onto sapphire to look into the magnetic properties of Fe(1 1 0) thin films, a buffer layer has always been used [5,10,11]. To our knowledge, only Metoki et al. looked at the structural and magnetic properties of Fe on *a*-axis (1 1–2 0) sapphire without using a buffer layer [12,13]. It was found that Fe(1 1 0) films on

*Corresponding author. Tel.: +32-16-327195; fax: +32-16-327983.

E-mail address: johan.swerts@fys.kuleuven.ac.be (J. Swerts).

0040-6090/02/$ - see front matter
PII: S0040-6090(02)00247-X

sapphire form three domains and that they exhibit a strong in-plane uniaxial anisotropy.

In Fe_xCo_{1-x} bulk alloys and thin films, the particular composition $x=40$ leads to a negative K_1 value and this influences profoundly the in-plane magnetic anisotropy. We show that in our case the structural and magnetic properties of the Fe films and the $Fe_{40}Co_{60}$ films grown on *a*-axis (1 1−2 0) sapphire are similar to each other. The orientation of the bcc Fe and $Fe_{40}Co_{60}$ films on Al_2O_3(1 1−2 0) is (1 1 0), they both display a strong uniaxial in-plane anisotropy and they exhibit a comparable thickness dependence of the coercive field along the easy axis i.e. when the magnetization reversal process is dominated by domain wall nucleation and motion. We have evaluated this dependence using the results of the structural characterization. Hence in this article, the interplay between the structural and magnetic properties of thin Fe and $Fe_{40}Co_{60}$ films on *a*-axis (1 1−2 0) sapphire without buffer layer is discussed.

2. Experimental details

Fe and $Fe_{40}Co_{60}$ films were grown by molecular beam epitaxy (MBE) onto single crystal *a*-axis (1 1−2 0) sapphire substrates at various temperatures. The base pressure during deposition in the MBE chamber is $\approx 10^{-10}$ mbar. The substrates were degassed by annealing them for 30 min at $T=950$ °C. The Fe films were deposited by e-beam evaporation and the $Fe_{40}Co_{60}$ alloys were prepared by co-deposition from two independently controlled e-beam guns. The e-beam guns are controlled by quadrupole mass spectrometer systems. The evaporation rates were calibrated by quartz crystal oscillators and X-ray reflectivity measurements. The Fe films were grown at a rate of 0.45 Å/s and the evaporation rates of Fe and Co during co-deposition were 0.18 and 0.27 Å/s, respectively. The film thickness was varied from 5 to 60 nm. Protective Ag layers with a thickness of 2 nm were deposited on top of the Fe and $Fe_{40}Co_{60}$ films. The quality of the films has been checked in situ by reflection high-energy electron diffraction and ex situ by X-ray diffraction (XRD) and was optimised by varying the substrate temperature during deposition. We find that Fe and $Fe_{40}Co_{60}$ films deposited on sapphire at a substrate temperature $T_s=300$ °C develop a good crystalline quality.

The X-ray measurements presented in this paper are obtained with θ−2θ scans on a Rigaku diffractometer with a 12 kW rotating anode and using a pyrolitic graphite single crystal monochromator to select Cu Kα radiation ($\lambda=0.154$ nm). The step size of the measured data was 0.01°.

The surface study is performed on a commercial atomic force microscope (M5, Park Scientific Instruments).

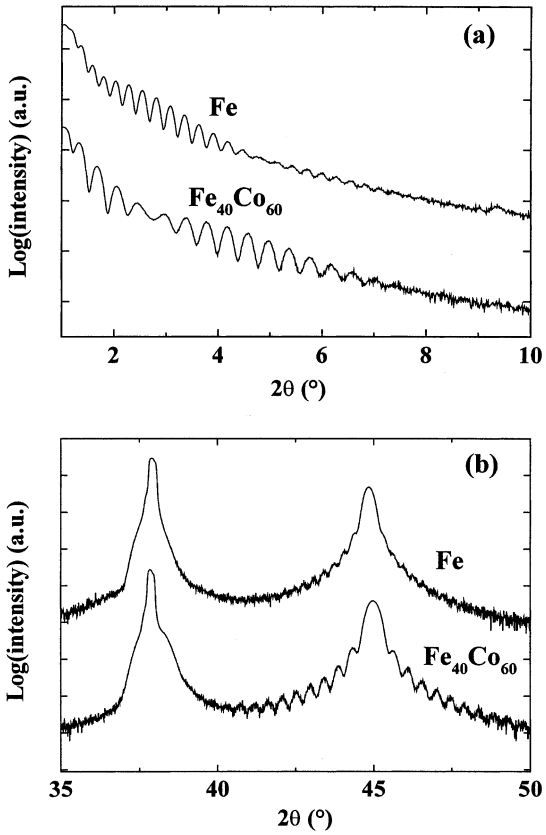

Fig. 1. XRD profiles for the Fe (upper curve) and $Fe_{40}Co_{60}$ (lower curve) films at (a) low angles and (b) high angles. The curves have been offset vertically for clarity.

The magnetic properties of the samples were characterized ex situ by using the longitudinal magneto-optical Kerr effect (MOKE). The MOKE system consists of a polarized HeNe 10 mW laser source operating at 632.8 nm, two polarizers, a Faraday modulation coil, and a photodetector. Magnetization measurements in the longitudinal geometry were carried out in two configurations. In the first configuration the magnetic field is applied parallel to the film surface and to the plane of incidence in order to determine the in-plane component of magnetization parallel to the applied field. In the second configuration the applied field is parallel to the film surface but perpendicular to the plane of incidence in order to measure the in-plane component of magnetization perpendicular to the applied field.

3. Structural characterization

3.1. X-ray diffraction

After preparation, the Fe and $Fe_{40}Co_{60}$ films were taken out of the vacuum system for the XRD measurements. For both compositions, Fe and $Fe_{40}Co_{60}$, a typical film is considered.

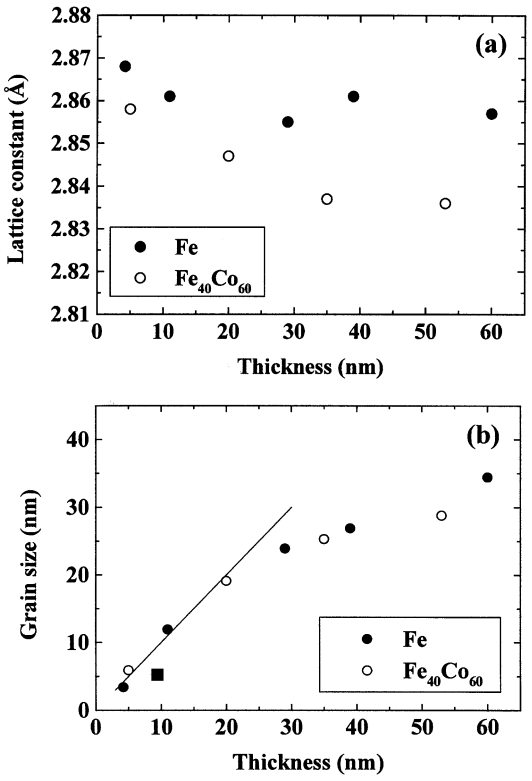

Fig. 2. (a) Lattice constant for Fe and $Fe_{40}Co_{60}$ films vs. film thickness; (b) Perpendicular coherence length vs. film thickness for Fe and $Fe_{40}Co_{60}$ films.

Fig. 1 shows the low (a) and high (b) angle XRD scans of a 27 nm thick Fe film (upper curve) and a 20 nm $Fe_{40}Co_{60}$ (lower curve) film. For clarity, the curves have been shifted vertically with respect to each other. The low-angle profiles allow calculating the film thickness. The high-angle diffraction profile consists of 2 peaks: the left peak is caused by the (1 1−2 0) plane of the sapphire substrate, while the right one corresponds to the main reflection from the (1 1 0) planes of the magnetic film. The presence of finite size peaks in the high-angle profile confirms that both films have a rather limited roughness. The thickness calculated from the high-angle profiles is consistent with the calculated thickness using the low-angle profiles.

Fig. 2a shows the average lattice parameter vs. film thickness obtained from the high-angle XRD measurements. The lattice constant of the $Fe_{40}Co_{60}$ alloys exhibits a relaxation towards a value 2.835 Å corresponding to the calculated value for the bulk alloy using Végard's law. Our experimental value, 2.835 Å, is also in agreement with the value obtained for bulk alloys of the same composition [14]. Hence we can assume that there is a larger strain present in the thinner films whereas in the thicker films a relaxation of the lattice constant occurs. Internal strain may influence the magnetic anisotropy of the films [11].

Information about the perpendicular crystalline coherence length can be obtained with Scherrer's law. This coherence length, in general, is limited to the perpendicular grain size. It should be noted that Scherrer's law might lead to a small overestimate, especially for thinner films. In Fig. 2b the perpendicular coherence length vs. film thickness for the Fe and $Fe_{40}Co_{60}$ films is plotted. The full line corresponds to a grain size equal to the film thickness. It is clear that below 30 nm the films have a structural coherence length of almost 100% of the total film thickness. For the thicker films the grain size tends to saturate. The structural coherence length will be less than the total film thickness. Hence, there will be relatively more grain boundaries present in the thicker films when compared to the thinner films. These grain boundaries can act as pinning sites for magnetic domain walls.

3.2. Atomic force microscopy

Magnetization reversal in thin films is strongly influenced by the surface roughness [15,16]. Therefore the surface roughness of the $Fe_{40}Co_{60}$ alloys for different thickness was evaluated ex situ by atomic force microscopy (AFM) in order to correlate their morphology to the magnetization measurements. Scanning probe microscopy is well suited to obtain quantitative information about surface roughness and its dependence on lateral length scale [17,18].

For the purpose of these roughness measurements, three samples of different thickness were prepared simultaneously by sliding a mask across the sample holder. Fig. 3a shows a typical AFM top view of a 500 nm by 500 nm area of a 5 nm thick $Fe_{40}Co_{60}$ thin film. The vertical interface width, determined by the root mean square (rms) roughness σ, characterizes the surface roughness along the vertical direction. The $Fe_{40}Co_{60}$ rms roughness at different length scales (0.5–5 μm) is plotted vs. thickness in Fig. 3b. As is seen on this graph, the rms roughness value increases as the thickness of the samples increases for all length scales.

4. Magnetic characterization

4.1. Magnetic anisotropy

The in-plane magnetic anisotropy of the bcc Fe and bcc $Fe_{40}Co_{60}$ films has been studied in detail by varying the orientation of the magnetic field with respect to the crystallographic directions in steps of 5° or 15°. Fig. 4 shows for both compositions the angular dependence M_R/M_S of the normalized remanent parallel magnetization in the longitudinal geometry. The Fe and $Fe_{40}Co_{60}$ films are, respectively, 60 and 53 nm thick. The data for both samples exhibit cosine-like polar plots, showing that a simple uniaxial anisotropy is consistent with the

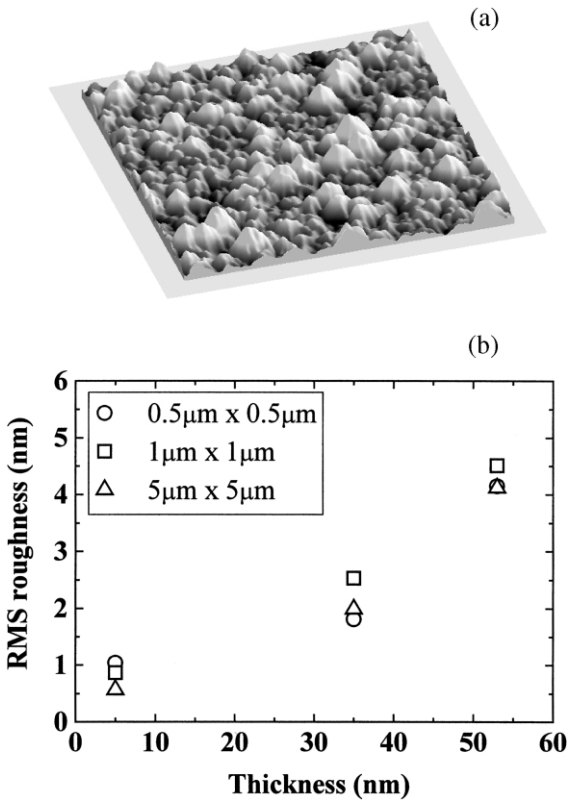

Fig. 3. (a) AFM micrograph of the surface of a 5 nm $Fe_{40}Co_{60}$ film for an area of 500 nm by 500 nm. The black to white contrast is 3 nm; (b) evolution of the rms roughness as a function of sample thickness derived from the AFM measurements on the $Fe_{40}Co_{60}$ alloys on various length scales.

magnetic anisotropy of our Fe and $Fe_{40}Co_{60}$ films. Contrary to the expectations, we have observed that the in-plane anisotropy of all the investigated Fe and $Fe_{40}Co_{60}$ films are similar to each other due to the presence of a dominant uniaxial anisotropy. Hence, a change of sign of the first anisotropy constant K_1 could not be observed. The precise orientation of the easy axis with respect to crystallographic directions of the substrate is not clear yet. The easy axis is not oriented consistently 80° (or −10° for samples thicker than 26 nm) away from the $Al_2O_3[0\,0\,0\,1]$ axis as determined by Metoki et al. This inconsistence can be due to the different preparation technique and growth conditions. Moreover, the fact that Fe films form three domains probably enhances the sensitivity to the experimental conditions. Further investigation is needed to clarify this issue.

4.2. Magnetization reversal

As shown by Daboo et al. [19,20] the magnetization reversal process can be studied in more detail by comparing the magnetization components parallel and perpendicular to the applied field. In our films with uniaxial anisotropy the reversal process should be rather simple. Fig. 5 shows three MOKE loops of the transverse magnetization of a 39 nm thick Fe film. The inset in each graph shows the parallel component of magnetization. When the magnetic field is applied close to the easy axis (Fig. 5a), no transverse magnetization is measured, corresponding to a 'single-jump' switching process. This indicates that the switching behaviour is dominated by domain wall motion. When the magnetic field is applied perpendicular to the easy axis, the reversal is mainly achieved through rotation. This is illustrated in Fig. 5b. When the field is applied in any other direction the reversal process will be a combination of both mechanisms as is shown in Fig. 5c. In this case

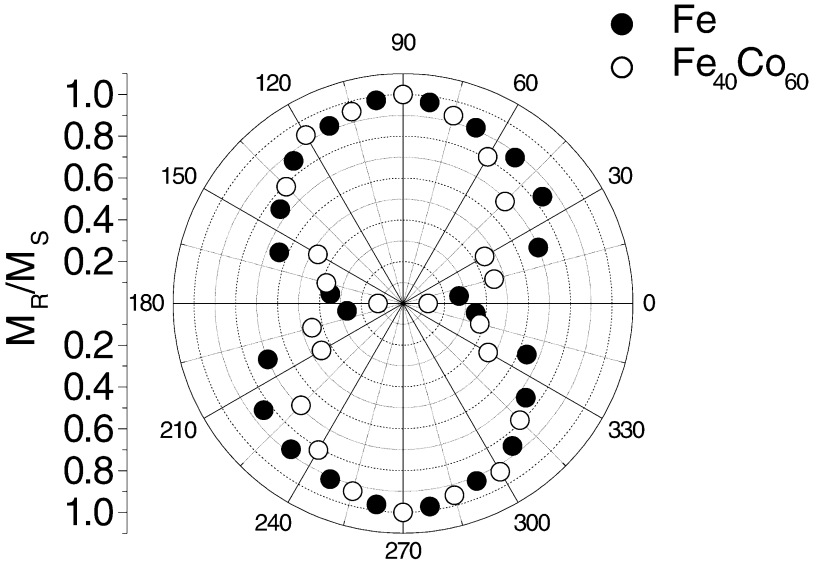

Fig. 4. Polar plot of the normalized in-plane remanent magnetization M_R/M_S for a 60 nm Fe thin film (●) and a 53 nm $Fe_{40}Co_{60}$ thin film (○).

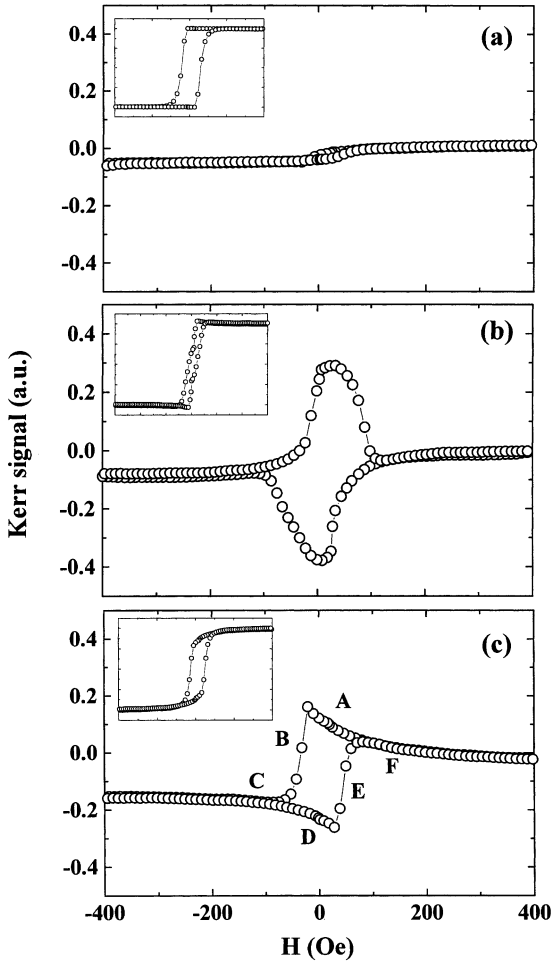

Fig. 5. Measurements of the in-plane transverse component of the magnetization of a 39 nm Fe film; (a) with the applied field along the easy axis; (b) perpendicular to the easy axis; and (c) 30° away from the easy axis. The insets of the graphs show the corresponding measurements of the parallel magnetization component.

the field is applied 30° away from the easy axis. The magnetization first rotates away from saturation field direction towards the easy axis (A, D) then switches along the easy axis (B, E) and finally rotates again towards reversed saturation field direction (C, F). These measurements confirm the conclusion that a uniaxial anisotropy characterizes the anisotropy of our samples and give information about the orientational dependence of the magnetization reversal process. Similar results are obtained for the $Fe_{40}Co_{60}$ films.

In the following we will concentrate on the magnetic reversal process when the applied field is along the easy axis of magnetization. The dominant switching mechanism is in this case reversal by domain wall motion. In view of the rectangular shape of the hysteresis loop along an easy axis, the coercive field H_c will be equal to the so-called switching field at which the reversal process commences. In Fig. 6, a study of the coercive field along the easy axis vs. sample thickness is shown. The dotted line is a guide for the eye. Both the systems reveal comparable thickness dependence. The coercive field increases with film thickness except for the 5-nm thick films that show an unexpected high coercivity (50 Oe).

5. Discussion

Domain wall motion in a thin metal film can be described as a domain wall that propagates in an energy landscape. The shape of this landscape is influenced by the presence of grain boundaries, inclusions, surface roughness and other defects. Hence, potential barriers and potential minima, so-called pinning sites, are being formed that inhibit the nucleation or propagation of the domain wall. To overcome the barrier or to remove the domain wall from such a pinning site, external energy needs to be supplied e.g. by applying a magnetic field. In this case the coercive field is a good measure of this extra energy. The difficulty is to distinguish which defect is responsible for an enhanced coercivity.

The structural characterization with XRD and AFM led to the following results: (i) the lattice parameter shows a relaxation with increasing thickness towards a value that is consistent with bulk values; (ii) the grain size (in a direction perpendicular to the sample) scales with the thickness for thinner films but tends to saturate for thicker films. Consequently, relatively more grain boundaries will be present as the film thickness increases; (iii) the rms roughness of the samples increases as their thickness increases.

The first result indicates that the thinnest films exhibit a large internal strain. If this strain is inhomogeneous, the magnetic anisotropy will be influenced by this strain and the resulting strain fields may deform the potential landscape and enhance the nucleation field and consequently the coercivity. Since the Fe(1 1 0) film is stiffer in the [1−1 0] direction than in the [0 0 1] direction,

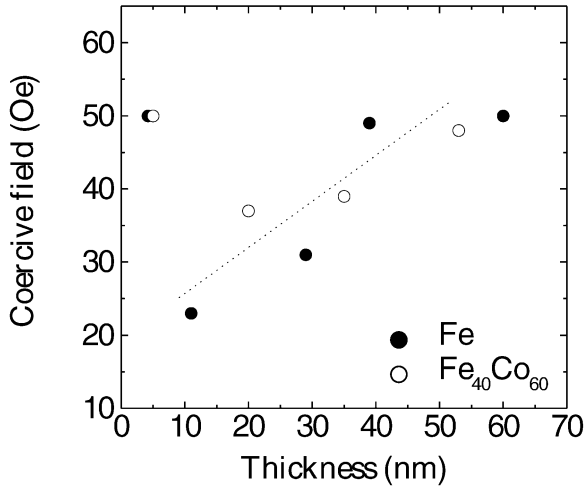

Fig. 6. Coercive field vs. sample thickness with the magnetic field applied along the easy axis. Fe films (●) and $Fe_{40}Co_{60}$ films (○). The dotted line is a guide for the eye.

inhomogeneous strain is favoured. The second result leads to the following conclusion: the thicker the samples, the smaller the structural coherence, the larger the number of grain boundaries becomes. Since each grain boundary can act as a local barrier, the coercive field will increase as the thickness of the samples increases. The third result is also consistent with an increased coercivity with increasing thickness, since enhanced surface roughness can also inhibit domain wall nucleation and motion.

Our interpretation is consistent with the measured thickness dependence of the coercive field in the Fe as well as in the $Fe_{40}Co_{60}$ thin films. Although the roughness is small and the structural coherence length is large in the thinnest films (5 nm), these films exhibit a rather unexpected high coercive field. This could be caused by the large internal strain. Another effect that could be involved, is the oxidation of the metals on sapphire substrates [12,21]. Oxidation of the Fe atoms close to the sapphire interface can cause strong interface anisotropy and consequently can enhance the coercivity. Since the oxidation process is an interface effect and since the internal strain is reduced in the thicker films, surface roughness and structural coherence start to dominate the domain wall nucleation and motion processes. This implies in our case an increased coercivity with increasing film thickness.

6. Conclusions

We have grown Fe(1 1 0) and $Fe_{40}Co_{60}$(1 1 0) thin films on single crystal *a*-axis (1 1−2 0) sapphire substrates without any buffer layer. The structural properties are investigated with XRD and AFM measurements. MOKE measurements show that the Fe films as well as the $Fe_{40}Co_{60}$ alloy films have a uniaxial anisotropy. Both systems reveal a strong thickness dependence of the coercive field with the applied field along the easy axis. We have evaluated this dependence using the results of the structural characterization. The results show that in the thicker films larger coercivity is due to the enhanced roughness and increased number of grain boundaries. The thinnest films exhibit an unexpected large coercivity that is probably caused by large internal strain or an interfacial oxidation process.

Acknowledgments

This work has been supported by the Fund for Scientific Research-Flanders (FWO), the Belgian IUAP, and the Flemish GOA programs. K.T. is a Post-Doctoral Research Fellow of the FWO.

References

[1] J. de Boeck, G. Borghs, Phys. World (1999) 27.
[2] R.C. Hall, J. Appl. Phys. 31 (1960) 157S.
[3] C.J. Gutierrez, J.J. Krebs, G.A. Prinz, Appl. Phys. Lett. 61 (1992) 2476.
[4] Th. Mühge, Th. Zeidler, Q. Wang, Ch. Morawe, N. Metoki, H. Zabel, J. Appl. Phys. 77 (1995) 1055.
[5] Yu.V. Goryunov, I.A. Garifullin, Th. Mühge, H. Zabel, JETP 88 (1999) 377.
[6] J.H. Dunn, D. Arvanitis, N. Martensson, J. Phys. IV 7 (1997) 383.
[7] M. Maurer, J.C. Ousset, M.F. Ravet, M. Piecuch, Europhys. Lett. 9 (1989) 803.
[8] F. Scheurer, B. Carriere, J.P. Deville, E. Beaurepaire, Surf. Sci. Lett. 245 (1991) 175.
[9] T. Nishizawa, K. Ishida, Bull. Alloy Phase Diagrams 5 (1984) 250.
[10] A.D. Kent, U. Ruediger, J. Yu, S. Zhang, P.M. Levy, Y. Zhong, S.S.P. Parkin, IEEE Trans. Magn. MAG-34 (1998) 900.
[11] B.M. Clemens, R. Osgood, A.P. Payne, B.M. Lairson, S. Brennan, R.L. White, W.D. Nix, J. Magn. Magn. Mat. 121 (1993) 37.
[12] N. Metoki, M. Hofelich, Th. Zeidler, T. Mühge, Ch. Morawe, H. Zabel, J. Magn. Magn. Mat. 121 (1993) 137.
[13] T. Mühge, A. Stierle, N. Metoki, H. Zabel, U. Pietsch, Appl. Phys. A 59 (1994) 659.
[14] W.C. Ellis, E.S. Greiner, Trans. Am. Soc. Met. 29 (1941) 415.
[15] Y.-L. He, G.-C. Wang, J. Appl. Phys. 76 (1994) 6446.
[16] M. Li, Y.-P. Zhao, G.-C. Wang, H.-G. Min, J. Appl. Phys. 83 (1998) 6287.
[17] J. Krim, I. Heyvaert, C. Van Haesendonck, Y. Bruynseraede, Phys. Rev. Lett. 70 (1993) 57.
[18] K. Temst, M.J. Van Bael, B. Wuyts, C. Van Haesendonck, Y. Bruynseraede, D.G. de Groot, N. Koeman, R. Griessen, Appl. Phys. Lett. 67 (1995) 3429.
[19] C. Daboo, J.A.C. Bland, R.J. Hicken, A.J.R. Ives, M.J. Baird, M.J. Walker, J. Appl. Phys. 73 (1993) 6368.
[20] C. Daboo, R.J. Hicken, E. Gu, M. Gester, S.J. Gray, D.E.P. Eley, E. Ahmad, J.A.C. Bland, Phys. Rev. B 51 (1995) 15964.
[21] N. Metoki, Th. Zeidler, A. Stierle, K. Bröhl, H. Zabel, J. Magn. Magn. Mater. 118 (1993) 57.